Feasibility assessment of the interactive use of a Monte Carlo algorithm in treatment planning for intraoperative electron radiation therapy

Pedro Guerra[1,2]**, José M Udías**[3]**, Elena Herranz**[3]**,
Juan Antonio Santos-Miranda**[4,5]**, Joaquín L Herraiz**[3]**,
Manlio F Valdivieso**[6]**, Raúl Rodríguez**[6]**, Juan A Calama**[7]**,
Javier Pascau**[8,9]**, Felipe A Calvo**[4,5]**, Carlos Illana**[6]**,
María J Ledesma-Carbayo**[1,2] **and Andrés Santos**[1,2]

[1] Department of Electronic Engineering, ETSI Telecomunicación, Universidad Politécnica de Madrid, CEI Moncloa, 28040 Madrid, Spain
[2] Biomedical Research Center in Bioengineering, Biomaterials and Nanomedicine (CIBER-BBN), Spain
[3] Nuclear Physics Group (GFN) at the Atomic, Molecular and Nuclear Physics Department, Universidad Complutense de Madrid, CEI Moncloa, 28040 Madrid, Spain
[4] Departamento de Oncología, Hospital General Universitario 'Gregorio Marañón', Madrid, Spain
[5] Facultad de Medicina, Universidad Complutense de Madrid, CEI Moncloa, 28040 Madrid, Spain
[6] GMV SA, Calle Isaac Newton 11 (PTM), 28760 Tres Cantos, Madrid, Spain
[7] Department of Radiation Oncology, Clínica La Luz, Calle General Rodrigo 8, 28003 Madrid, Spain
[8] Departamento de Bioingeniería e Ingeniería Aeroespacial, Universidad Carlos III de Madrid, Avda. de la Universidad 30, 28911 Leganés, Spain
[9] Instituto de Investigación Sanitaria Gregorio Marañón, calle Doctor Esquerdo 46, 28007 Madrid, Spain

E-mail: pedro.guerra@upm.es

Abstract

This work analysed the feasibility of using a fast, customized Monte Carlo (MC) method to perform accurate computation of dose distributions during pre- and intraplanning of intraoperative electron radiation therapy (IOERT) procedures. The MC method that was implemented, which has been integrated into a specific innovative simulation and planning tool, is able to simulate the fate of thousands of particles per second, and it was

the aim of this work to determine the level of interactivity that could be achieved. The planning workflow enabled calibration of the imaging and treatment equipment, as well as manipulation of the surgical frame and insertion of the protection shields around the organs at risk and other beam modifiers. In this way, the multidisciplinary team involved in IOERT has all the tools necessary to perform complex MC dosage simulations adapted to their equipment in an efficient and transparent way. To assess the accuracy and reliability of this MC technique, dose distributions for a monoenergetic source were compared with those obtained using a general-purpose software package used widely in medical physics applications. Once accuracy of the underlying simulator was confirmed, a clinical accelerator was modelled and experimental measurements in water were conducted. A comparison was made with the output from the simulator to identify the conditions under which accurate dose estimations could be obtained in less than 3 min, which is the threshold imposed to allow for interactive use of the tool in treatment planning. Finally, a clinically relevant scenario, namely early-stage breast cancer treatment, was simulated with pre- and intraoperative volumes to verify that it was feasible to use the MC tool intraoperatively and to adjust dose delivery based on the simulation output, without compromising accuracy. The workflow provided a satisfactory model of the treatment head and the imaging system, enabling proper configuration of the treatment planning system and providing good accuracy in the dosage simulation.

(Some figures may appear in colour only in the online journal)

1. Introduction

Intraoperative electron radiation therapy (IOERT) refers to the delivery during surgery of a high dose of radiation, in a single session, directly to the post-resected tumour bed or to an unresected tumour. The dose to be delivered is usually prescribed in combination with external radiotherapy and/or chemotherapy, although it can occasionally be prescribed without any additional irradiation (Gunderson *et al* 2011).

Radiotherapy planning in IOERT is a complex task that requires the consensus of a multidisciplinary team to manage a given case. In this context, new tools have been proposed (Pascau *et al* 2012) for the study of different treatment alternatives during preplanning before surgery. Moreover, the ultimate decisions about cone dimensions or protection positioning are made during the final procedure, depending on the surgical findings: e.g. tumour size, resection margins, etc (Lamanna *et al* 2012). These last-minute modifications might require re-evaluation of the dose during surgery for quality control prior to dose delivery, a process that we will refer to as intraplanning.

In IOERT, Monte Carlo (MC) techniques have been mostly used to analyse the dosimetric characteristics of electron beams generated by the accelerator (Iaccarino *et al* 2011, Righi *et al* 2013) and to measure the influence of protection on dose delivery in phantom studies (Russo *et al* 2012). Nevertheless, the actual irradiation conditions in the operating room (OR) may differ significantly from those considered during simulations or phantom tests. Therefore,

there are compelling reasons to include aspects such as irregularities of the surface being treated or the accumulation of biological fluids in the estimation of dose homogeneity and distribution (Rosi and Viti 2004). The translation of previous research into clinical practice has been limited because of the complexity and time-consuming numerical computations typically associated with MC methods.

To plan the intervention with the aid of a treatment planning system (TPS), the radio-oncologist (RO), in co-operation with the surgeon, should allow the definition of plausible scenarios that could be found during the OR and simulate alternative treatments to define the best trade-off in each situation. Alternatively, the RO might be required to take into account the actual conditions in the OR and to recompute during surgery the dose distribution, before the dose is actually delivered. This is possible with the aid of an intraoperative CT and a tracking system (García-Vázquez *et al* 2013). In practice, to be useful in a clinical environment, the tool has to be accurate while allowing for a certain level of interactivity in performing both pre- and intraoperative dose computations, and this requirement imposes hard constraints on the computation time.

Despite its potential value, treatment planning in the context of IOERT has not been possible until recently, with the development of a specific TPS (*radiance,* GMV SA, Tres Cantos, Spain). It is believed that the lack of such a tool has limited the spread and acceptance of IOERT (Palta *et al* 1995). The TPS front-end allows region contouring, definition of the surgical frame and the representation of isodoses with the corresponding dose-volume histograms, based on the scenario being considered for dose delivery (Pascau *et al* 2012).

The ultimate goal of the framework around the TPS is to provide a flexible environment that enables accurate dose estimates within a period of a few minutes for any given CT volume of a patient, either pre- or intraoperatively, and for a given LINAC, either conventional or mobile.

This work analyses the capability of the IOERT TPS back-end for fast predictions of dose distributions during the clinical routine using optimized MC techniques, including irregularities and protection systems in the irradiation field. These capabilities are illustrated with two early breast cancer case studies, one showing application of the tool with preoperative images and the other with intraoperative images. Dose distributions were simulated by considering a standard configuration for this treatment: 5 cm applicator and 6 MeV electron beam nominal energy.

2. Material and methods

The simulation framework, whose workflow is shown in figure 1, provided the means to calibrate the imaging equipment, model the treatment unit, including the applicator, and simulate any situation that could be found in the OR, while hiding the complexity of the set-up to the end user. This allowed the users to concentrate on the decisions required for proper treatment: beam energy, applicator configuration and protection positioning. The phase space (PHSP) was generated using experimental measurements with phantoms, as described later. A CT phantom was imaged to calibrate the imaging equipment and thus enable the transformation of Hounsfield numbers into tissue properties. With the aid of the TPS, the user could insert objects not present in the original CT to account for the actual settings of the treatment plan. Using all of this information, the MC module computed the delivered dose.

These calibration steps have been validated with the clinical set-up available at Clinica la Luz (Madrid, Spain), consisting of an Mx8000 IDT 16 CT Scanner (Koninklijke Philips
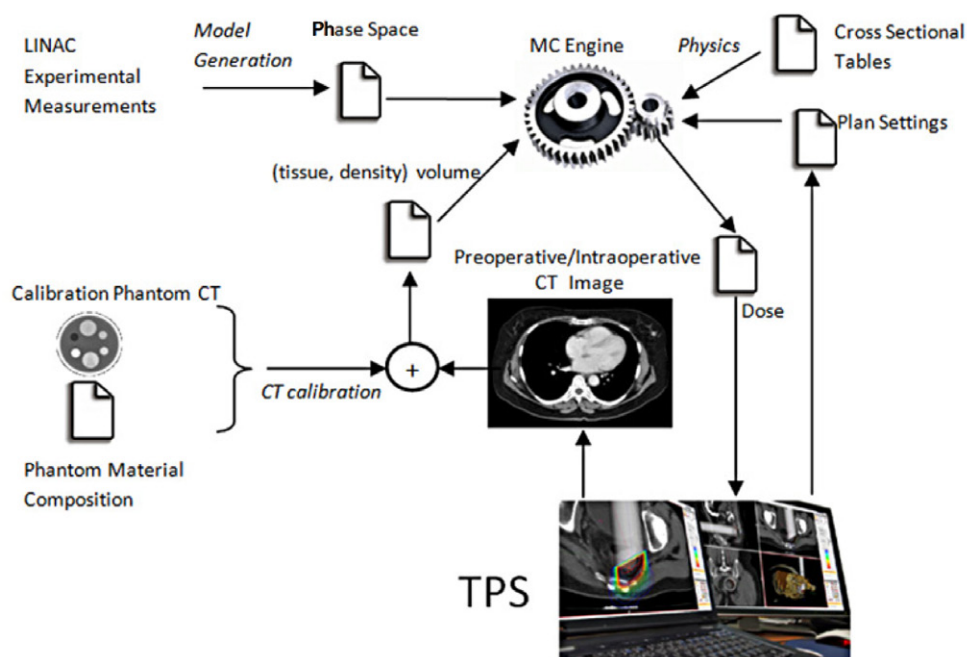
Figure 1. Technical workflow including configuration and user execution steps of the MC dose estimator included in the TPS system.

Electronics N.V., Amsterdam, The Netherlands) and a Varian 21EX linear accelerator (Varian Medical Systems, Palo Alto, CA, USA).

2.1. Treatment unit simulation

The physical properties of the electron beam for each energy and applicator diameter are characterized in the form of a PHSP model defined at a plane normal to the geometrical axis of the applicator. The PHSP describes the properties of the beam as a combination of multiple annular electron sources with nominal energy E_i and radius R_i, radiating along a line defined by the PHSP plane at the angles (θ_i, φ_i) (Herranz 2013). A weight factor w_i established the contribution of each elemental source to the beam. The model for the treatment unit, i.e. the computation of the individual weights w_i, was generated using a robust iterative maximum likelihood expectation maximization method (Herranz *et al* 2013), which provided a plausible set of weights for the existing experimental measurements. The iterative procedure consisted of two main steps: forward and backward projection. The forward projection provides, by the principle of linear superposition of doses, the dose D^{model} produced by the current PHSP as a weighted linear combination of the individual dose footprints d_i generated by each elemental source. The measured dose D^{exp} was then compared with D^{model}, and correction factors were obtained for each voxel of the volume being considered. The correction factor for each bin is computed based on the ratio of measured to modelled dose.

To efficiently generate particles out of the PHSP during simulation, elemental sources were sorted and stratified based on the value of their individual weight factors. The n_1 microsources with the highest weight factor values w_i belong to the first cluster, and similarly for the other

microsources. The number of microsources n_j in the cluster C_j was selected so that it had a predefined *a priori* probability *Pj*.

$$C_j = \{w_{s_j} \ldots w_{s_j+n_j}\}, \ \forall \ (i \ < \ k): w_i \geq w_k$$

$$P_j = \sum_{i=s_j}^{s_{j+1}-1} w_i \tag{1}$$

The actual source k was selected in two steps. Firstly, a random uniform number was generated to select the cluster j, and then a random element k was taken from the subset C_j using the rejection function $r(k)$.

$$r(k) = \frac{w_k}{\max\{w_k\}} > \ \eta, \ w_k \in C_j$$

$$\eta: : U(0, 1) \tag{2}$$

Particle variables (E, θ, φ) were generated randomly based on the nominal value of the randomly selected microsource k and the discretization binning $(\Delta E, \Delta \theta, \Delta \varphi)$. Particle position (x, y) in the PHSP plane was sampled directly from a ring with nominal radius R_k using the following expressions:

$$\xi :: U(0, 1), \varsigma :: U(0, 1)$$

$$r_2 = R_k + \frac{\Delta R}{2}, r_1 = R_k - \frac{\Delta R}{2}$$

$$\left. \begin{array}{l} \theta = 2\pi\varsigma \\ \rho = \sqrt{r_1 \cdot r_1 \cdot (1 - \xi) + r_2 \cdot r_2 \cdot \xi} \end{array} \right\} \begin{array}{l} x = \rho \cdot \cos(\theta) \\ y = \rho \cdot \sin(\theta) \end{array} \tag{3}$$

The PHSP was located above the exit plane of the applicator in a plane normal to its geometrical axis. The applicator was inserted in the volume as a methacrylate hollow cylinder, as shown in figure 2, overriding any material information coming from the CT image. With this approach, the effect of the bevel on the dose became part of the simulation, reducing the number of PHSP models to a single plane per nominal energy level and applicator diameter.

2.2. Imaging equipment calibration

Each voxel of the simulation volume was automatically assigned a tissue type and a density using a stoichiometric method (Schneider *et al* 1996, Vanderstraeten *et al* 2007) that generated device-specific conversion tables with the aid of a calibration phantom. In our implementation, model fitting was achieved by a constrained nonlinear multivariable optimization that searched for the set of cross-section values (K_{ph}, K_{coh}, K_{KN}) that minimized the maximum error between the model and the observed Hounsfield values in the calibration phantom. Constraints were imposed to avoid the convergence of cross-section fitting constants into negative values observed in the original algorithm (Kock and Schreuder 1996). Non-constrained results may provide a good fit but have no physical meaning.

A calibration phantom was acquired with an Mx8000 CT Scanner to validate the model-fitting algorithm developed for the scanner calibration. For this scanner, the algorithm provided the fitting constants: $K_{ph}/K_{KN} = 1.001 \times 10^{-8}$ and $K_{coh}/K_{KN} = 1.212 \times 10^{-5}$. These values provided the relationship between simulation tissues and Hounsfield values for this particular machine.
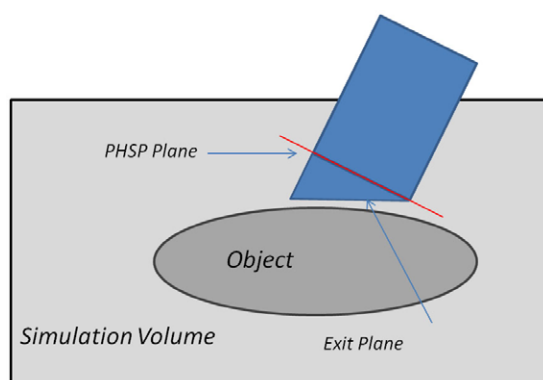
Figure 2. Diagram for the simulation of bevelled applicators.

2.3. Protection and bolus insertion

ROs need to define the expected surgical frame on the TPS by removing the tissues that will be resected or displaced during surgery from the simulation volume, as well as including new elements not found in the CT volume but present during dose delivery. Beam modifiers, such as bolus, are placed at the end of the applicator or on the patient surface, and shielding is used to protect critical structures (Beddar *et al* 2006). Twelve different protection materials, including lead, brass, aluminium and polymethyl methacrylate, among others, are currently available to define protection shields.

Protection systems and modifiers are 3D structures for which the user needs to specify dimension, orientation, shape and coordinates in the volume. During the planning procedure, these structures are inserted in the simulation volume, overriding the local tissue type and density given by the CT for each voxel and replacing it with the corresponding material type.

2.4. MC dose estimation

Dose to the medium was computed using a custom implementation of the dose planning method (DPM) (Sempau *et al* 2000), a 'mixed' class algorithm that runs in a fraction of the time of the original computer program. DPM uses an analogue simulation of photon interactions and a class II condensed history method (Kawrakow and Bielajew 1998) for electron simulation, treating large energy-transfer collisions in an analogue sense and using the continuous slowing-down approximation (CSDA) to model small energy-loss collisions. Cross-sections and mean free paths for each energy and material type were computed and tabulated offline. During simulation, these physical parameters were estimated by interpolation.

In our implementation, computational acceleration is achieved by optimizing the algorithm flow and efficiently using the hardware resources available in a modern multicore computer. The graphic processor unit, which can also be used to speed up the computation of dose (Jia *et al* 2011, Hissoiny and Ozell 2011), is devoted to image rendering in the TPS.

2.4.1. Parallelization. Particle transport is inherently a parallel problem and, therefore, porting the algorithm onto a multicore architecture was relatively straightforward. Execution is divided into threads, each simulating a subset of the total number of particles. To avoid any overhead due to synchronization, threads are loosely coupled. That is, just read-only data

structures were shared, and there is a single common critical section to monitor conditions for stopping the simulation.

2.4.2. Algorithm.   With respect to electrons, our implementation incorporates a dual random hinge approach (Bielajew and Wilderman 2000), in which energy loss and multiple elastic scattering are fully decoupled. Additionally, the management of secondary particles below cut-off values is changed in the simulator engine to prevent their insertion into the simulation queue, thus reducing the workload. Random numbers are generated using a re-entrant combination of linear generators (L'Ecuyer 1998), which are efficient to execute while being sufficiently random to pass demanding statistical tests (L'Ecuyer and Hellekalek 1998, L'Ecuyer and Panneton 2005).With respect to photons, Compton scattering is the main mechanism for dose delivery at the energies under consideration. Photoelectric absorption is relevant at low energies and for high atomic numbers. Pair production becomes significant at the high end of the energy range and for materials with high atomic numbers. Photon transport is implemented following the δ-scattering method (Sempau *et al* 2000). In the standard approach, a sequence of Compton interactions ends with either a photoelectric interaction or a pair production. In our implementation, both interactions were forced, i.e. a fraction of the photon energy was absorbed as a photoelectric interaction and another fraction produces an electron/positron pair. The fraction that undergoes each process depended on the relative probability of each interaction at the given photon energy.

2.4.3. Compiler.   Iterative loops are reordered and unrolled to reduce the use of conditional branches, thus avoiding costly pipeline flushes. Pointers are de-aliased at function calls to provide the compiler with more freedom in code reordering and optimization.

2.4.4. Hardware.   Particles are generated and simulated in blocks to increase data and code locality, and to improve throughput. The memory layout of interpolation spline coefficients is arranged to have them stored in consecutive memory positions, so that they are fetched from external memory in a single access and stored in a single cache line, thus reducing the number of memory accesses and cache misses.

The statistical uncertainty of the simulated dose is determined using the history-by-history method (Walters *et al* 2002), which provides the estimated uncertainty σ_j^2 for each voxel as:

$$\sigma_j^2 = \frac{1}{N-1} \left(\frac{\sum_{i=1}^N D_i^2}{N} - \left(\frac{\sum_{i=1}^N D_i}{N} \right)^2 \right), \tag{4}$$

where N is the number of simulated histories and D_i is the deposited dose per voxel. Periodically during the simulation, the maximum uncertainty is calculated for those voxels whose dose is higher than 50% of the maximum dose (D_{max}). Simulation execution ends when the maximum uncertainty is lower than a value specified by the user, which in our simulations was usually set to 2%.

At the end of the simulation, the worst-case uncertainty σ_{max}^2 is calculated for those voxels where the dose was higher than 50% of D_{max}. Simulation efficiency ε, is defined as

$$\varepsilon = \frac{1}{\sigma_{max}^2 T}, \tag{5}$$

where T is the CPU time required to run the simulation, is reported after every simulation.

2.5. Dose verification

The accuracy of the underlying algorithm to reproduce dose distributions, obtained either by using other MC codes (Sempau *et al* 2000) or measured experimentally (Chetty *et al* 2007), has already been shown by other authors. However, the proposed implementation introduces multiple optimizations and modifications that had to be verified.

The verification of dose distributions was performed in three steps. First, DOSRZnrc (Kawrakow and Rogers 2000), which is widely used by the medical physics community for the calculation of dose deposition, was used as a reference to assess the accuracy of the MC simulation. Second, experimental measurements in a water tank were compared with simulated dose profiles using a PHSP model of the accelerator obtained with our iterative method. Finally, monitor units (MU) required to deliver a given prescribed dose with different bevel angles and field sizes were computed following the standard protocol used in the clinic, and these values were compared with the dose profiles obtained using the MC method.

Dose distributions for a monochromatic parallel source, with beam energy between 4 and 20 MeV, in water and slab phantoms were simulated to compare our MC simulation with DOSRZnrc. Two alternative slab phantoms, consisting of water, aluminium and lung, were used to stress the code with a high-energy beam and a sharp inhomogeneity (Rogers and Mohan 2000).

PHSP models for the Varian 21EX system, with nominal energy in the 6–20 MeV range and an applicator diameter of 6 cm, were generated using the iterative method described in section 2.1. For each energy, a PHSP model was estimated using water measurements with a right-angled applicator. The 6 cm applicator was used as an example to show the capability of reproducing dose distributions at different energies and bevel angles. The computation of dose footprints d_i was carried out offline in a computer cluster, with a computational effort equivalent to 10 months of a single-core processor. Once the dose footprints were computed, the iterative algorithm found a set of weights fitting the estimated dose to the measured dose in water for this specific accelerator. A full iteration of the fitting algorithm was completed when the multiplicative factor had been computed for all bins, and all bins in the PHSP were updated using these factors. The entire fitting procedure typically required around 200 full iterations before convergence, which took a few minutes to fit each energy and cone diameter using a single-core processor.

MC simulations were then used to obtain the number of MUs required to deliver a given prescribed dose with different bevel angles and energies, and these values were compared with those obtained through measurement and hand computation (Cygler *et al* 1997).

Following the recommendations of the Spanish Medical Physics Society, absorbed dose to water protocols were used for calibration (IAEA2000). Relative measurements were taken in water and air with an MP3 radiation field analyser (PTW, Freiburg, Germany), equipped with a *p*-type electron diode detector (Scanditronix Medical AB, Uppsala, Sweden). Another diode detector was placed in the periphery of the radiation field during scanning to acquire reference conditions. The TANDEM electrometer (PTW) was used for all scanning measurements. The uncertainty of such a measurement protocol is less than 1% in dose and 0.5 mm in distance. *P*-type electron diodes were also used to measure cone output factors in water (Björk *et al* 2004), with an uncertainty lower than 0.5%.

MUs were calibrated for each energy to provide 1 cGy at the maximum of the percentage depth dose (PDD) in water, per MU, with the standard 10 cm × 10 cm applicator and a source-to-surface distance (SSD) of 100 cm. Output factors (OF) were computed (Almods 1999) at the maximum of the clinical axis with three different SSDs for each
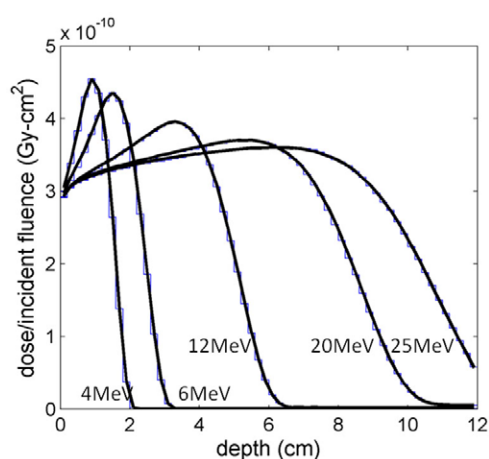
Figure 3. PDD results for a broad mono-energetic electron beam with nominal energies in the range of 4–25 MeV, computed with the implemented MC code (solid-black) and DOSZRnrc (dashed-blue).

bevel-diameter combination and intermediate distances were estimated by interpolation, taking a 10 cm × 10 cm applicator as a reference. To estimate MU with the MC method, a gain factor was computed for each PHSP so that the simulation output was in the same units as the water measurements. In this way, MUs were estimated for a 127 cm applicator using the OFs computed previously.

3. Validation and results

All calculations reported here were performed on a PC running Microsoft 64-bit Windows 7 with an Intel 2.93 GHz i7 processor and 8 GB RAM.

3.1. Dose simulation with monochromatic sources

Dose–depth profiles in a water phantom (figure 3) and slab phantoms (figures 4 and 5) were simulated using a monoenergetic beam at different energies. Dose profiles in water of figure 3 confirmed agreement between the reference (DOSRZnrc) and computed profiles, with a difference between curves lower than 1.5% of the maximum dose at max.

The slab phantom used in figure 4 demonstrate the accuracy of the MC model to reproduce dose profiles in the energy range of interest for procedures with protection around the lung, with a relative error below 1.5%. Additionally, the slab phantom described in figure 5 was used to stress the code with a high-energy beam and a sharp inhomogeneity (Rogers and Mohan 2000). The results show good agreement between the profiles, with a slight mismatch along the lung. In fact, this mismatch was smaller than that found using the original computer program (Sempau *et al* 2000), as shown in the upper-right corner of the figure 5. The differences were attributed to the use of a finer grid for the precomputed cross-sections, as well as to the algorithmic changes introduced.

These results show that the MC method implemented accurately predicted dose profiles in the presence of sharp inhomogeneities, which is a common scenario in IOERT where high atomic number (Z) materials are used to shield organs at risk. In addition, the
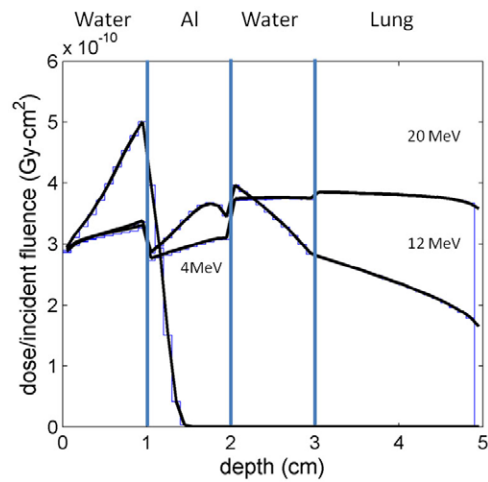
Figure 4. PDD in a 5 cm water/aluminium/water/lung the slab phantom for a broad mono-energetic electron beam with nominal energies in the range of 4–20 MeV, computed with the implemented MC code (solid-black) and DOSZRnrc (dashed-blue).
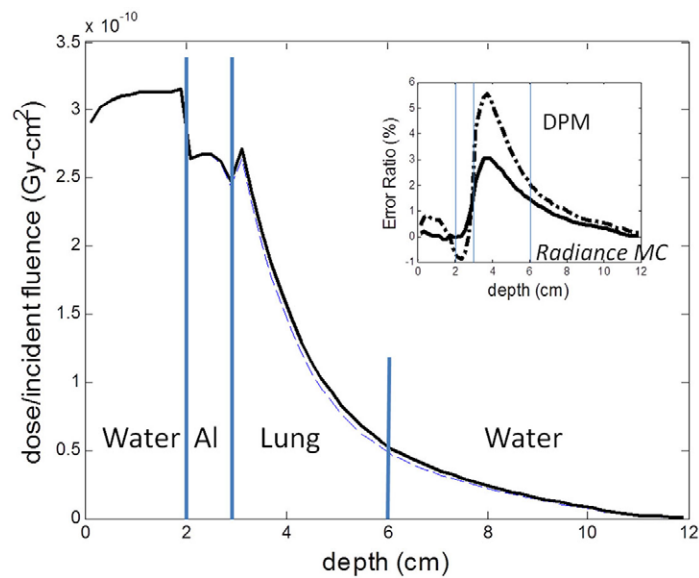
Figure 5. Comparison of depth-dose curve in a water/al/lung/water slab phantom for 1.5 × 1.5 cm² 20 MeV mono-energetic electron beam, radiating from a uniform point source at 100 cm incident on the phantom, computed with the implemented MC code (solid black) and DOSRZnrc (dashed-blue). The relative error with respect to the reference is shown in the upper right corner for the MC code (solid black) and the original implementation of the algorithm (dashed black). Simulations are run with the cutoff energies 200 keV and 50 keV energy for electrons and photos, respectively.
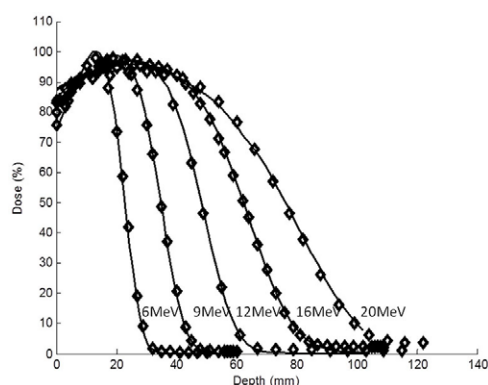
Figure 6. Simulated (solid) and measured (diamonds) PDD curve for a 6 cm applicator at nominal head energies of 6, 9, 12, 16, and 20 MeV.

computations required a fraction of the time needed by the original computer program, as discussed in section 3.3.

3.2. Treatment unit simulation results

Figure 6 compares the experimental and simulated PDD curves for a 6 cm right-angled applicator for nominal energies between 6–20 MeV, while figure 7 compares the experimental and simulated lateral profiles at 16 MeV for a 6 cm bevelled applicator, with bevel angles between 15° and 45°. Figure 7 shows the ability to model the effect of the bevel and to predict the shape of the lateral dose profiles. The fact that measurements with bevelled applicators were not employed to fit the PHSP must be taken into account, and thus they are a good indicator of the validity of the PHSP + MC algorithm for this configuration. However, the ability to reproduce measurements depends greatly on the PHSP model, and, therefore, a complete validation of the iterative methods used to model the phase space is required; such a study falls beyond the scope of this work and has been addressed by (Herranz *et al* 2013).

The gamma function (Low *et al* 1998) was used to compare the experimental profiles with the simulation output for all energies and bevel angles, with the result that the gamma function was smaller than that corresponding to a dose difference of 3% and to estimating distance to an agreement of 3 mm, which is well within the needs of IOERT.

As a further test of the suitability of the MC + PHSP for this case, MUs were measured and computed for dose distributions in a water phantom with an SSD of 127 cm and bevels of 0°, 15°, 30° and 45° to verify that the resulting values could be trusted. Table 1 summarizes the required number of MUs estimated by the MC tool for each energy and bevel, and enabled comparison of this value with manually computed MUs using the measurement data.

The ratio between values calculated by the MC tool and the measurements confirmed their consistency, with a mean value of 1.004 and a standard deviation of 0.013 for the 6 cm applicator. By averaging these values for all measured applicator diameters (3, 4, 5, 6, 7, 8 and 9 cm), the mean value of the ratio was 0.999 and the standard deviation was 0.016, values that are comparable with those reported by other authors (Cygler *et al* 2004) for electron beams with a different MC-calculation engine.
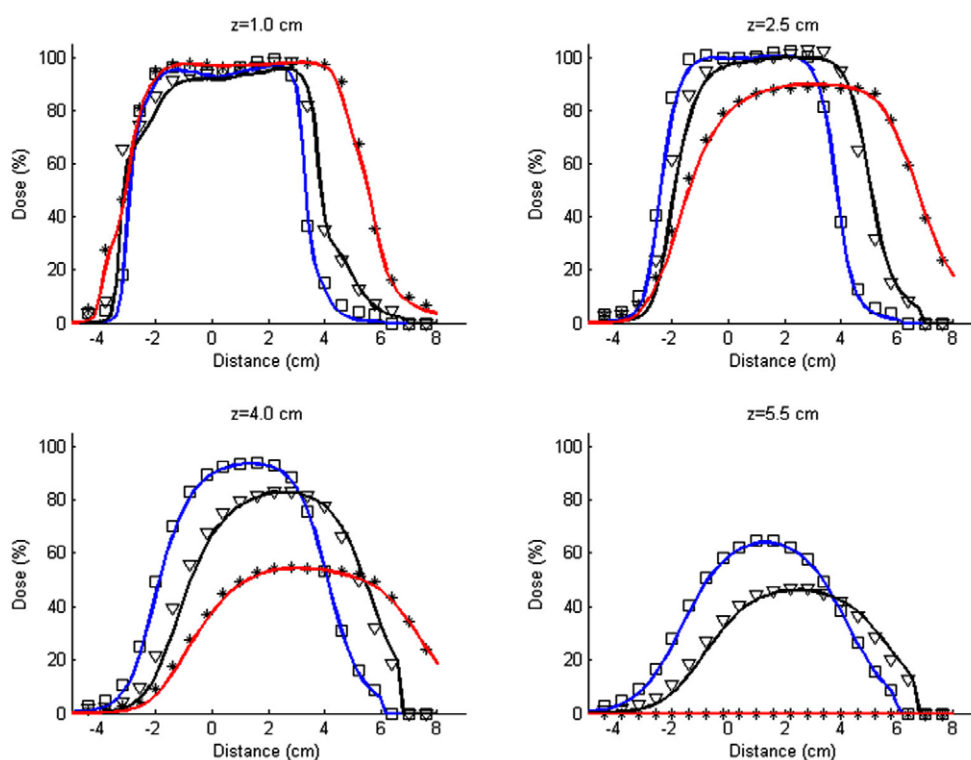
Figure 7. Simulated (solid line) and measured (scattered points) lateral dose for a 6 cm applicator at nominal head energy of 16 MeV and bevels of 15º (blue-square), 30º (black-diamond) and 45º (red-star) at depths equal to 1 cm, 2.5 cm, 4 cm and 5.5 cm.

3.3. Algorithm optimization and profiling

The algorithm was profiled to identify and progressively optimize bottlenecks. Particular attention was paid to the generation of random numbers and the sampling of different probability density functions, portions of code used intensively in the MC.

The actual load distribution depends on the object being modelled, as well as the energy and applicator size. With the aim of reducing the computation time in worst-case scenarios, only configurations with wide applicators and high energy were considered for code profiling. The distribution of workload in a water phantom with an 8 cm applicator at 20 MeV, summarized in table 2, is very similar to the distribution in the reference implementation of the algorithm (Sempau *et al* 2000). Simulation effort was divided into four main modules: particle generation, simulation management, particle transport and energy recording. The simulation of electron physics took most of the computational effort (71.7%). The simulation of electrons was split into the implementation of the CSDA and the simulation of discrete events, such as the generation of bremsstrahlung photons. In both cases, the computational effort was divided into the actual transport of particles within the volume (geometry) and statistical sampling of the different physical processes to compute displacement and rotation angles.

The sampling of the PHSP was costly without stratification. Four layers were enough to reduce the effort of particle generation from 30% to 3.9% of the total simulation time. Moreover, random number generation, which was used at multiple points, accounting for

Table 1. Comparison of MU Monte Carlo versus measurements for all nominal energies and bevels for an applicator diameter of 6 cm, for a prescribed dose of 21 Gy at d_{max} along the beam central axis.

Bevel	6 MeV		9 MeV		12 MeV		16 MeV		20 MeV	
	MC	MC/Meas	MC	MC/Meas	MC	MC/Meas	MC	MC/Meas	MC	MC/Meas
0	4215	1.006	3018	0.995	2692	0.998	2596	0.998	2596	1.001
15	4322	0.986	3118	0.997	2750	0.995	2612	0.995	2612	0.999
30	4462	1.004	3164	1.010	2765	1.005	2607	1.010	2566	1.009
45	4467	0.989	3110	1.001	2749	1.020	2595	1.026	2606	1.044

Table 2. MC code profiling for an 8 cm applicator in a water phantom for a 20 MeV source, expressed as percentage of the total simulation time.

MC simulation step				Percentage of total time
Particle Generation				3.9%
Particle Matter Interactions	Electrons (71.7%)	CSDA	Geometry	19.1%
			Physics Sampling	33%
		Discrete Electrons	Geometry	3.4%
			Physics Sampling	16.2%
	Photons (1.8%)			1.8%
Energy Tallying				18.3%
MC Simulation Manager				2.1%
Other				2.2%

12% of the computing time. This fact justifies the use of an efficient re-entrant combination of linear generators.

To assess the impact of the different modifications introduced to the original implementation, the efficiency gain provided by the MC tool in every run was evaluated for a fixed number of particles after algorithmic improvements (CODE OPT), memory layout and compiler considerations (MEM OPT) and simulation parallelization into multiple threads (THREAD). These values were compared with the efficiency of original code. The results, summarized in figure 8, show that the efficiency doubled after algorithmic and memory optimizations, and an additional factor of four was achieved by execution on multicore architecture. Because the underlying physics were the same, the efficiency gains were due mostly to a reduction in the computation time.

The motivation behind these optimizations was the intention to use the TPS and the MC to perform treatment preplanning and intraplanning. The intraoperative simulation helps to take into consideration the actual setting in the operating room and to validate hypotheses assumed during planning before the actual delivery. In clinical practice, where the patient is anaesthetized and undergoing surgery, the aim is that the MC computation should not delay the procedure, and it is necessary that the simulation be completed in less than 3 min. In dose simulations with a water phantom with $1 \times 1 \times 1 \text{ mm}^3$ voxels, it was observed (figure 9) that such a restrictive time constraint was not met when wide applicators and high energies were used, even for a relatively lax uncertainty requirement of 4% of the dose at the maximum, which required the simulation of more than 30 million particles.
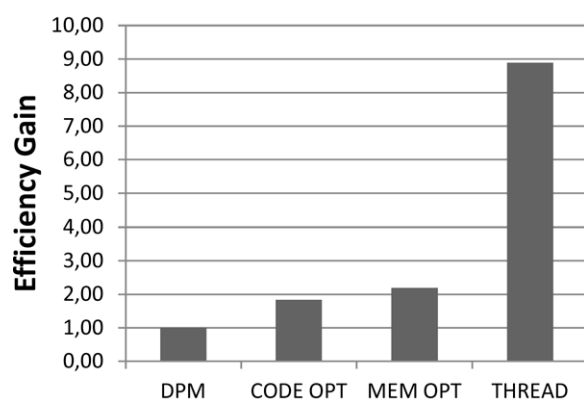
Figure 8. Efficiency gain for the original code running on 1 core (DPM), the optimized algorithm (CODE OPT) running on 1 core, the former algorithm with the new memory layout and compiler-oriented optimizations (MEM OPT) running on 1 core, and finally with execution divided into 6 threads (THREAD), running on 4 cores. Simulations are run in a $3 \times 3 \times 3\,mm^3$ voxelized water phantom with a 20 MeV monochromatic source.

In figure 9 it is observed that, if we restrict ourselves to the combinations used most frequently in clinics (where energies above 12 MeV are rarely used) and consider a larger voxel size ($8\,mm^3$ instead of $1\,mm^3$), accurate dose distributions, with uncertainties lower than 2%, could be completed in less than 3 min in most scenarios.

3.4. Dose simulations with the complete workflow

Two representative scenarios of treatment planning in breast cancer are presented to illustrate the utility and limitations of the workflow that was developed and implemented. In case 1, the preoperative image would typically be used to analyse possible treatment approaches. In case 2, the intraoperative CT image would be used to confirm whether the actual set-up in the operating room, including the applicator and position of the protection, meets the prescribed requirements before dose delivery.

CT studies were acquired at Hospital Gregorio Marañón in Madrid on a Toshiba Aquilion LB scanner (Toshiba Medical Systems Corporation, Tochigi, Japan) with the following parameters: voltage 120 KVp, current 40 mA, slice thickness 3 mm and pixel spacing $1.8 \times 1.8\,mm^2$ for case 1, and slice thickness 5 mm and pixel spacing $1 \times 1\,mm^2$ for case 2. The intraoperative CT was obtained as part of a research protocol in which a specifically designed couch was used to transport the patient from the OR to the CT scanner under anaesthesia, with the applicator treatment position fixed using an articulated arm. This protocol was designed to evaluate the difficulties and contributions of intraoperative CT imaging in IOERT scenarios. The optimal clinical protocol definition is still under investigation.

Case 1 emulates a preplanning workflow. In this scenario, the RO would use the preoperative image to segment the planning target volume (PTV), organs at risk and fluids on the tumour bed; select the treatment configuration (applicator position, diameter and bevel angle, as well as the nominal energy); and place the beam modifiers depending on several factors (size of the treatment target, anatomical structures, candidate areas to be protected). In this simulated scenario, shown in figure 10, the RO would prescribe 21 Gy to irradiate the PTV around the tumour bed delineated as a truncated cone shape, with a base of 40 mm and a height of 15 mm. The user, in this particular case an RO with IOERT experience following
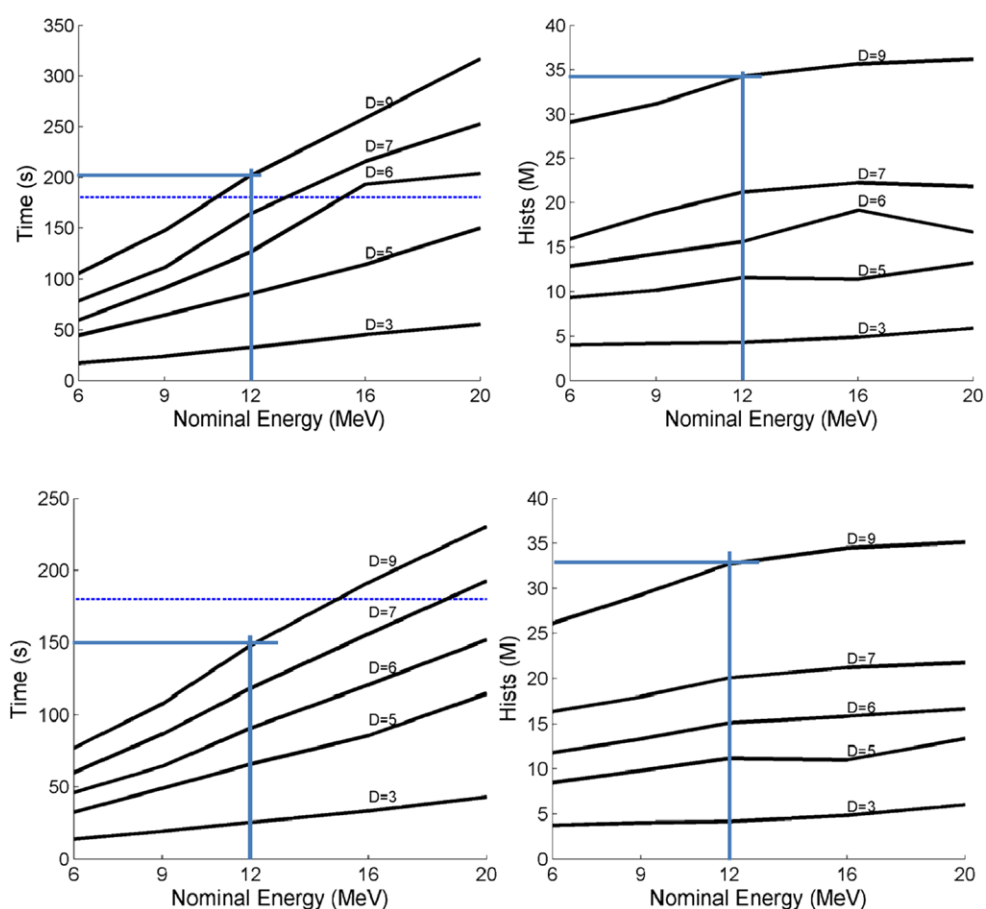
Figure 9. (Upper-left) Simulation time required to estimate dose with an uncertainty lower than 4% for a 161 × 140 × 161 water phantom, with 1 × 1 × 1 mm^3 per voxel and for applicator diameters in the range of 3 cm–9 cm. (Upper-right) Number of simulated primary particles in millions. (Lower-left) Simulation time required to estimate dose with an uncertainty lower than 2% for the same phantom with a 2 × 2 × 2 mm^3 voxelization and (lower-right) the required number of simulated primary particles.

the standard clinical protocol that he follows in the OR, positioned a 5 cm diameter applicator and inserted an 8 cm diameter/5 mm thick cylindrical shield (3 mm aluminium/2 mm brass) at the location where he considered that the ribs and lung would be best protected. With these settings, the RO and the radiation physicist expected to protect the lungs and ribs completely, while the delineated target volume would receive at least 90% of the prescribed dose. Multiple simulations, with slight variations in the applicator, protection positions and angles, were run to identify the optimal applicator location in terms of PTV coverage. This case used a two-layered disc configuration, which is frequently utilized in practice; the top disc with the lower *Z* slows down beam particles and absorbs backscattered particles (Catalano *et al* 2007), and the bottom disc with the higher *Z* stops the residual electrons.

Dose was estimated by considering a 6 MeV electron beam generated by a Varian 21EX linear accelerator. To obtain a statistical dose uncertainty $\sigma_{\max}^2$ below 2%, approximately
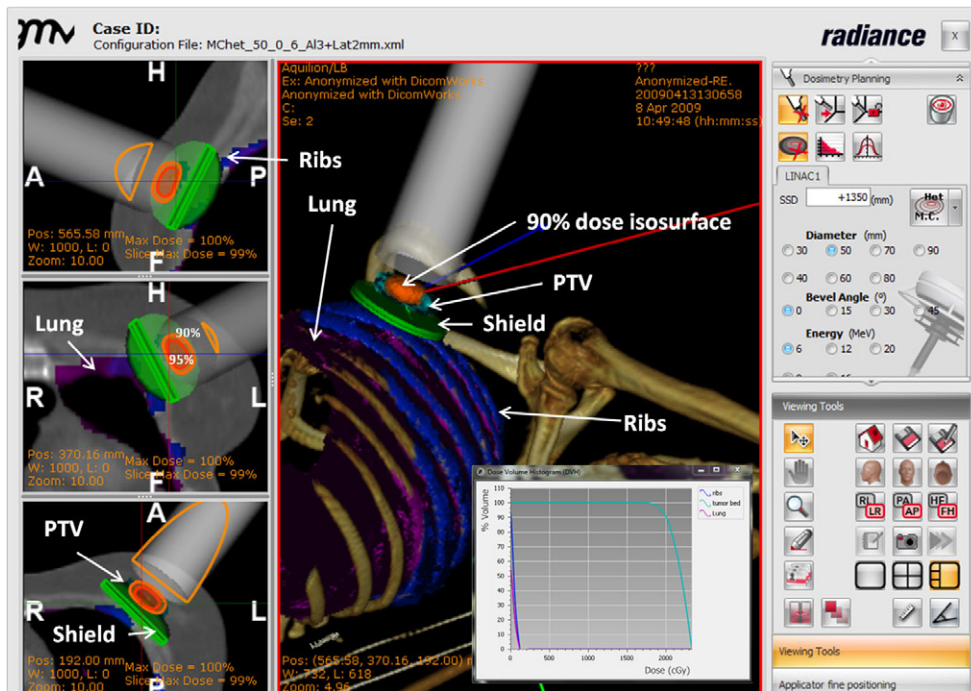
Figure 10. TPS interface showing the MC simulation output for a treatment planning with a 6 MeV electron beam and a 5 cm applicator (case 1). The breast is protected with a composite shield that is positioned by a RO. The pixel size of the preoperative CT image is $1.8 \times 1.8 \times 3\,\text{mm}^3$. Isodoses curves are represented for the 95% (red) and 90% (orange) of the maximum dose.

11.2 million particles, with an execution time of less than 35 s, were simulated in each MC run. This execution time would allow for a certain degree of interactivity in the planning process.

After several iterations, the RO determined that in the best-case scenario (figure 11, top left) the PTV was not completely enclosed by the 90%-isodose curve obtained with the 5 cm applicator, and it was estimated that, at best, 88% of the tumour volume was inside the 90%-isodose curve. The same setting was simulated with a 6 cm applicator (figure 11, top right), and in this case the delineated PTV was completely enclosed by the 90%-isodose curve, allowing for a margin of safety in the OR for position of the applicator and/or protection misalignments with respect to the optimum location. These simulation results are in accordance with the new standard treatment proposed by the European Institute of Oncology where the recommended applicator size is now 6 cm, with an occasional use of 5 cm for very small lesions (Dall'Oglio 2013).

In case 2, the applicator was placed in the TPS to reproduce the real applicator position, as displayed on the CT image (figure 12). The CT scan was obtained with the protection in place, although other clinical protocols for breast cancer treatment avoid the use of any protection (Fastner *et al* 2013). The reconstructed CT image showed severe artefacts due to the high density of the shielding materials. To simulate dose deposition, the applicator was positioned so that it overlapped the end of the applicator visible in the image, protection was placed on top of the protection with artefact visible on the image, and the tissue between the applicator and the protection was segmented as soft tissue. This workaround overcomes the limitations
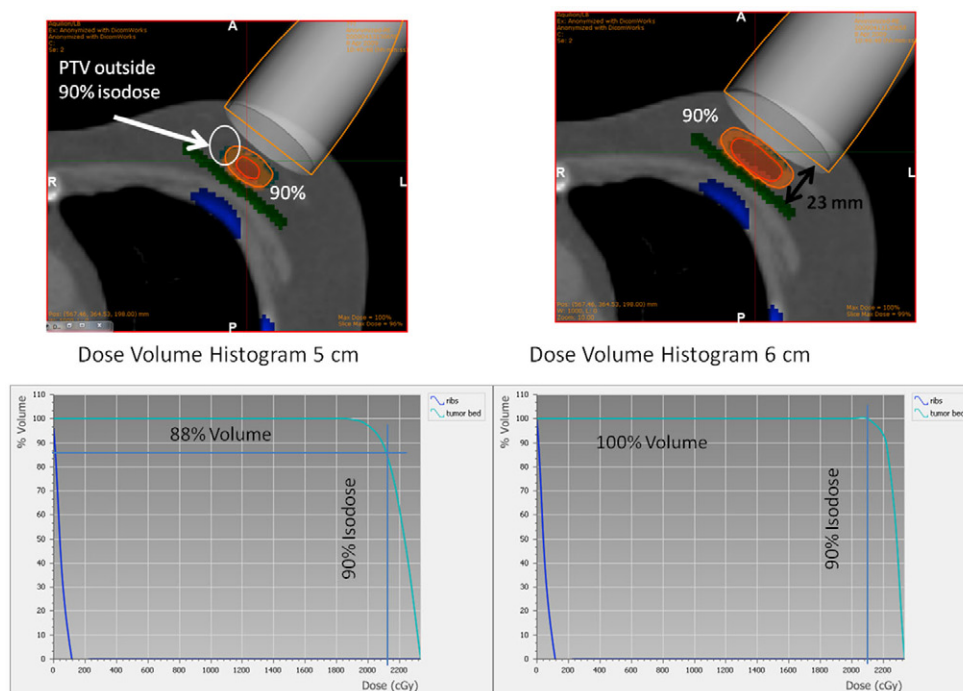
Figure 11. (Top) Representation of the 90% isodose curve for a 5 cm (top-left) and a 6 cm (top-right) applicator for case 1. An arrow is used to highlight poor coverage on the sides of the tumour bed. (Bottom) Representation of the corresponding DVH, where the vertical line represents 90% of the prescribed dose. Isodoses curves are represented for the 95% (red) and 90% (orange) of the maximum dose.

caused by the artefacts by replacing pixel values with the expected materials. However, the correspondence between the simulated dose and the actual delivered dose is uncertain. The simulation required 6.2 million histories and took 18 s to meet a 2% level of uncertainty. This computation time is small enough to not interfere with the surgical procedure.

4. Discussion and conclusions

This work has analysed the conditions under which a custom implementation of an existing MC algorithm meets the requirements for interactive use in IOERT during planning and treatment. The availability of an MC method capable of satisfying time and accuracy constraints in all scenarios would pave the way for systematic use of treatment planning in the IOERT clinical routine. The computation of volumetric distributions is a clear step forward with respect to reporting the 90%-dose curve and the maximum dose, which is currently the standard protocol (Beddar *et al* 2006).

As part of this work, the accuracy of the MC tool implemented to reproduce dose profiles in water and slab phantoms was assessed at different energies. These tests verified that the optimized algorithm was at least as accurate as the original implementation, even in the presence of sharp inhomogeneities, while requiring a fraction of the computation time.
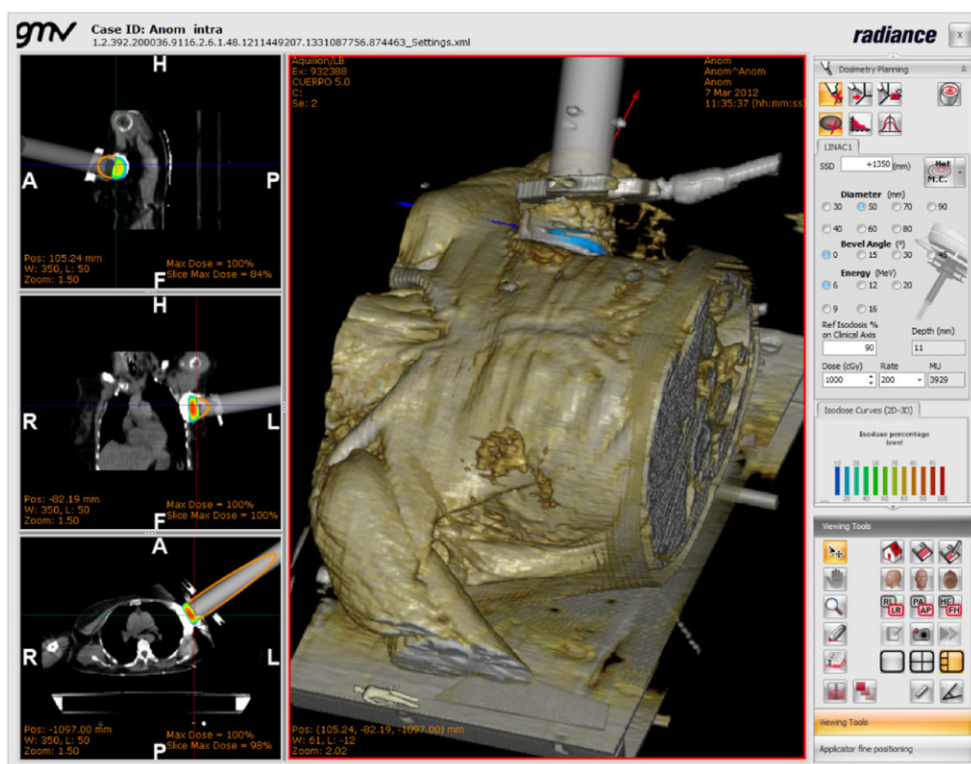
Figure 12. TPS interface showing the MC simulation output for an intraoperative treatment with a 6 MeV electron beam and a 5 cm applicator (case 2). The breast is protected with a composite shield by a RO and the applicator is kept in place by a holder. The pixel size of the intraoperative CT image is $1 \times 1 \times 5 \, \text{mm}^3$.

To assess the level of interactivity that can be expected, execution times to meet a predefined uncertainty level were evaluated using a collection of PHSPs capable of reproducing experimental measurements in a water phantom for nominal energies in the range of 6–20 MeV. From these simulations, it was concluded that all set-ups commonly used in the clinical routine could be solved in less than 2.5 min if the voxel size was kept above $2 \times 2 \times 2 \, \text{mm}^3$.

The actual level of interactivity that can be achieved has been illustrated with two early breast cancer test cases for which treatment plans had been defined, considering a 6 MeV beam energy and including protection around the lung. It is in this scenario where the use of a fast MC tool becomes more relevant; analytical methods, such as pencil beam, show serious limitations when inhomogeneous phantoms are evaluated because of high-density inhomogeneities and the use of a relatively low-energy electron beam (Ding *et al* 2005). Computation time is also a critical issue, particularly when the RO needs to simulate multiple alternatives or to confirm dose distributions for a given set-up in the OR. In both test case scenarios, the dose was computed in less than 35 s for an uncertainty lower than 2% of the dose at the maximum. These results confirm the interactive usability of this MC technique, without compromising accuracy in dose predictions, provided that the CT images used as input to the model are adequate for accurate dosimetry. Therefore, we may conclude that computation time or accuracy are no longer a bottleneck for the application of MC simulation in IOERT when used as an additional step for quality control and documentation of the procedure.

From the clinical perspective, the validity and usefulness of TPS has been assessed in a comparative study conducted with the participation of three ROs (Calvo *et al* 2014). Fifteen cases based on the most representative locations of IOERT treatments were evaluated, with the conclusion that the TPS offers a new imaging expansion for IOERT, in the context of a multidisciplinary approach to optimize and define the treatment parameters. However, the actual use of the TPS in the clinic requires the consideration and discussion of other factors. With regard to the use of the TPS with preoperative CT images, which is the planning workflow for IOERT that was originally proposed (Pascau *et al* 2012), the matter of the level of accuracy that can be obtained using preoperative images to estimate the actual dose distribution is a topic that is still under investigation, beyond the preliminary results given by (Pascau *et al* 2011).

Concerning the intraoperative use of the TPS, it is intuitive that this is the best approach to fully understand the patient's actual anatomy during treatment and should be considered if accurate dose estimations are intended. To obtain updated patient imaging during the IOERT procedure, portable devices should be considered in the protocol (Siewerdsen 2001). Nevertheless, several challenges, which are still being studied, must be taken into account to acquire and post-process such images. These include the effects of shielding disks on the image, the image quality and potential dosimetric limitations of portable CT devices or the methodology to transfer segmented regions and volumes from the preoperative to intraoperative images, in order to avoid manual segmentation by the RO in the time-constrained intraplanning phase. In any case, the MC workflow proposed here could assist in evaluating the potential use of a portable CT scanner for dose estimations in IOERT. The benefits of intraoperative imaging in the clinical workflow should also be confirmed for different treatment locations.

In IOERT, it is common to use a shielding disk to protect the organs at risk, but this introduces important artefacts in the CT that may limit the use of intraplanning. Further study of the sensitivity of dose distributions to these artefacts is needed, as well as investigating alternative techniques to minimize or remove them. In fact, the use of this MC tool in the TPS could be a valuable tool to assess the benefits and effects of different protection materials.

Finally, to minimize the delay in the procedure due to intraplanning computations, segmentation contours from preoperative images could be transferred to the intraoperative study by means of non-rigid image registration techniques.

The proposed MC-optimized tool and the workflow presented narrow the gap between external and internal radiotherapy, providing the RO with mechanisms to estimate the actual dose delivered to the patient in a complex clinical scenario, including the effects of protection systems and bolus. The integration of the MC tool in a user-friendly TPS will help in the standardization of IOERT and increase its applicability. Additionally, these techniques will enable improved handling of patients, an improved analysis of the treatment outcome, as well as a dose summation in those cases where IOERT is combined with external radiotherapy as a boost strategy.

Acknowledgments

References

Almond P R, Biggs P J, Coursey B M, Hanson W F, Huq M S, Nath R and Rogers D W O 1999 AAPM's TG-51 protocol for clinical reference dosimetry of high-energy photon and electron beams *Med. Phys.* **26** 1847–70

Beddar A S, Biggs P J, Chang S, Ezzell G A, Faddegon B A, Hensley F W and Mills M D 2006 Intraoperative radiation therapy using mobile electron linear accelerators: report of AAPM Radiation Therapy Committee Task Group No. 72 *Med. Phys.* **33** 1476–89

Bielajew A F and Wilderman S J 2000 Innovative electron transport methods in EGS5 *Proc. of the Second Int. Workshop on EGS4* (Japan: KEK Proceedings 2000–20) pp 1–10

Björk P, Knöös T and Nilsson P 2004 Measurements of output factors with different detector types and Monte Carlo calculations of stopping-power ratios for degraded electron beams *Phys. Med. Biol.* **49** 4493–506

Calvo F A, Murillo L A, Sallabanda M, Martinez-Villanueva J and Solea C V 2014 Imaging opportunities for treatment planning in intraoperative electron beam radiotherapy (IOERT): developments in the context of RADIANCE system *Rep. Pract. Oncol. Radiother.* **19** 239–45

Catalano M, Agosteo S, Moretti R and Andreoli S 2007 Monte Carlo simulation code in optimisation of the IntraOperative Radiation Therapy treatment with mobile dedicated accelerator *J. Phys.: Conf. Ser.* **74** 012002

Chetty I *et al* 2007 Report of the AAPM Task Group No. 105: issues associated with clinical implementation of Monte Carlo-based photon and electron external beam treatment planning *Med. Phys.* **34** 4818–53

Cygler J, Daskalov G, Chan G and Ding G 2004 Evaluation of the first commercial Monte Carlo dose calculation engine for electron beam treatment planning *Med. Phys.* **31** 142–53

Cygler J, Li X A, Ding G X and Lawrence E 1997 Practical approach to electron beam dosimetry at extended SSD *Phys. Med. Biol.* **42** 1505

Dall'Oglio S 2013 'Study protocol: electrons for intraoperative radiotherapy in selected breast-cancer patients: late results of the Montpellier phase II trial' *Radiat. Oncol.* **8** 191 Radiation Oncology, comments to the manuscript

Ding G, Cygler J, Yu C, Kalach N and Daskalo V G 2005 A comparison of electron beam dose calculation accuracy between treatment planning systems using either a pencil beam or a Monte Carlo algorithm *Int. J. Radiat. Oncol. Biol. Phys.* **63** 622–33

Fastner G *et al* 2013 IORT with electrons as boost strategy during breast conserving therapy in limited stage breast cancer: long term results of an ISIORT pooled analysis *Radiother. Oncol.* **108** 279–86

García-Vázquez V, Marinetto E, Santos-Miranda J A, Calvo F A, Desco M and Pascau J 2013 Feasibility of integrating a multi-camera optical tracking system in intra-operative electron radiation therapy scenarios *Phys. Med. Biol.* **58** 8769–82

Gunderson L L, Willett C G, Harrison L B and Calvo F A 2011 *Intraoperative Irradiation: Techniques and Results* (New York: Humana)

Herranz E 2013 Simulaciones Monte Carlo para Radioterapia Intraoperatoria con haces de electrones *PhD Thesis* Universidad Complutense, Madrid

Herranz E, Herraiz J L, Ibañez P, Perez-Liva M, Puebla R, Cal-Gozález J, Guerra P, Rodríguez R, Illana C and Udías J M 2013 Phase space determination of electron beam for intraoperative radiation therapy from measured dose data *Phys. Med. Biol.* Submitted

Hissoiny S and Ozell B 2011 GPUMCD: a new GPU-oriented Monte Carlo dose calculation platform *Med. Phys.* **38** 754–65

Iaccarino G, Strigari L, D'Andrea M, Bellesi L, Felici G, Ciccotelli A, Benassi M and Soriani A 2011 Monte Carlo simulation of electron beams generated by a 12 MeV dedicated mobile IORT accelerator *Phys. Med. Biol.* **56** 4579–96

Jia X, Gu X, Graves Y J, Folkerts M and Jiang S B 2011 GPU-based fast Monte Carlo simulation for radiotherapy dose calculation *Phys. Med. Biol.* **56** 7017–31

Kawrakow I and Bielajew A F 1998 On the condensed history technique for electron transport *Nucl. Instrum. Methods Phys. Res.* B **142** 253–80

Kawrakow I and Rogers D W 2000 The EGSnrc code system: Monte Carlo simulation of electron and photon transport *Technical Report PIRS-701* ed N R C o, Ottawa, Canada

Kock E A D and Schreuder A N 1996 Letters to the editor. Comments 'The calibration of CT Hounsfield units for radiotherapy treatment planning' *Phys. Med. Biol.* **41** 1524–7

L'Ecuyer P 1998 Tables of maximally equidistributed combined LFSR generators *Math. Comput.* **68** 261–9

L'Ecuyer P and Hellekalek P 1998 Random number generators: selection criteria and testing *Random and Quasi-Random Point Sets* (New York: Springer) pp 223–65

L'Ecuyer P and Panneton F 2005 Fast random number generators based on linear recurrences modulo 2: overview and comparison *Proc. of the Winter Simulation Conf.* (Orlando, FL: IEEE) p 10

Lamanna E, Gallo A, Russo F, Brancaccio R, Soriani A and Strigari L 2012 Intra-operative radiotherapy with electron beam *Modern Practices in Radiation Therapy* ed G Natanasabapathi (Rijeka: InTech)

Low D A, Harms W B, Mutic S and Purdy J A 1998 A technique for the quantitative evaluation of dose distributions *Med. Phys.* **25** 656–61

Palta J, Biggs P, Hazle J, Huq M, Dahl R, Ochran T, Soen J, Dobelbower R J and McCullough E 1995 Intraoperative electron beam radiation therapy: technique, dosimetry, and dose specification: report of task force 48 of the Radiation Therapy Committee, American Association of Physicists in Medicine *Int. J. Radiat. Oncol. Biol. Phys.* **33** 725–46

Pascau J, Santos Miranda J, Calvo F, Bouché A, Morillo V, González-San Segundo C, Ferrer C, López Tarjuelo J and Desco M 2012 An innovative tool for intraoperative electron beam radiotherapy simulation and planning: description and initial evaluation by radiation oncologists *Int. J. Radiat. Oncol. Biol. Phys.* **83** e287–95

Pascau J, Santos-Miranda J, San-Segundo C G, Illana C, Valdivieso M, García-Vazquez V, Marinetto E, Calvo F and Desco M 2011 Intraoperative Imaging in IOERT sarcoma treatment: initial experience in two clinical cases *Int. J. Radiat. Oncol. Biol. Phys.* **81** S90

Righi S, Karaj E, Felici G and Di Martino F 2013 Dosimetric characteristics of electron beams produced by two mobile accelerators, Novac7 and Liac, for IOERT through Monte Carlo simulation *J. Appl. Clin. Med. Phys.* **14** 3678

Rogers D W O and Mohan R 2000 Questions for comparison of clinical Monte Carlo codes *13th Int. Conf. the Use of Computers in Radiotherapy* ed W Schlegel and T Bortfeld (Heidelberg: Springer) pp 120–2

Rosi A and Viti V 2004 Guidelines for quality assurance in IOERT Oncología **27** 62–95

Russo G, Casarino C, Arnetta G, Candiano G, Stefano A, Alongi F, Borasi G, Messa C and Gilardi M C 2012 Dose distribution changes with shielding disc misalignments and wrong orientations in breast IOERT: a Monte Carlo—GEANT4 and experimental study *J. Appl. Clin. Med. Phys.* **13** 3817

Schneider U, Pedroni E and Lomax A 1996 The calibration of CT Hounsfield units for radiotherapy treatment planning *Phys. Med. Biol.* **41** 111–24

Sempau J, Wilderman S J and Bielajew A F 2000 DPM, a fast, accurate Monte Carlo code optimized for photon and electron radiotherapy treatment planning dose calculations *Phys. Med. Biol.* **45** 2263–91

Siewerdsen J H 2001 Cone-beam CT with a flat-panel detector: from image science to image-guided surgery *Nucl. Instrum. Methods Phys. Res.* A **648** S241–50

Vanderstraeten B *et al* 2007 Conversion of CT numbers into tissue parameters for Monte Carlo dose calculations: a multi-centre study *Phys. Med. Biol.* **52** 539–62

Walters B R B, Kawrakow I and Rogers D W O 2002 History by history statistical estimators in the BEAM code system *Med. Phys.* **29** 2745–52